

## Small Buoys for Energy Harvesting : Experimental and Numerical Modeling Studies

Stéphan T. Grilli<sup>1</sup>, Annette R. Grilli<sup>1</sup>, Steven P. Bastien<sup>2</sup>, Raymond B. Sepe Jr.<sup>2</sup>, and Malcolm L. Spaulding<sup>1</sup>

1. Department of Ocean Engineering, University of Rhode Island, Narragansett, RI, USA

2. Electro Standards Laboratories, Inc., Cranston, RI, USA

### ABSTRACT

We present the development and application of small buoy systems for wave energy harvesting (free-floating or slackly moored), to produce about 1 KW per unit at full scale. These systems are targeted for powering distributed marine surveillance and instrumentation networks, and should be simple in concept, easily deployable, storm resilient, and low maintenance. Our work involved design, experiments (both laboratory and field testing), and numerical simulations in realistic irregular wave climates, of two new types of buoy systems equipped with an embedded Linear Electric Generator (LEG; made of a permanent magnet, suspended to a spring, oscillating within a (two-phase) coil), whose armature motion is excited essentially by the buoy's wave-induced heave, with some effects of roll. The first design (DC2 buoy) has a spherical float, to which a cylindrical canister is rigidly attached, which houses the LEG. A rod, attached to the LEG magnetic armature, exits through the bottom of the canister and connects to a large submerged resistance platform (which also serves as ballast). The differential motion between the float and platform heave drives the LEG oscillations. By contrast, the second design (DC3) is a self-contained (water tight) resonating multiple-spar buoy (or *Starspar*), in which a longer central spar houses the LEG and is surrounded by shallower, satellite spars, providing both form stability and a reduced overall average draft (necessary to achieve a proper heave resonance period). The LEG, which has a large ballast simply attached to its bottom, oscillates as a result of buoy heave through coupled resonance. Hence, LEG oscillations are maximized by matching starspar heave and LEG natural periods, and both of these to the targeted sea state peak spectral period. For spar buoys, the former is simply controlled by buoy draft. Scale model experiments are performed

to calibrate numerical model parameters (essentially viscous drag coefficients), and select buoy characteristics to maximize energy production.

**KEYWORDS :** Wave energy systems; heaving buoy; linear electric generator; floating body dynamic; Boundary Integral Equations; linear waves; laboratory and field experiments.

### INTRODUCTION

Since 2006, as part of projects funded by ONR (SBIRs and STTRs), and the State of Rhode Island (STAC Alliance), the University of Rhode Island (URI) and Electro Standards Laboratories Inc. (ESL) have teamed up to work on the design, numerical simulation, and scale model and field testing of small buoy systems for omni-directional wave energy harvesting (free-floating or slackly moored). The targeted application for these systems is not large energy production for single units (except perhaps in a buoy farm configuration), but instead the development of simple, easily deployable, and storm resilient systems, to provide a renewable wave power source of ( $\mathcal{O}(1)$  kW for distributed marine surveillance and instrumentation systems (e.g., autonomous target recognition instruments, persistence and ubiquitous sensor systems, tracking and identification of maritime vessels, and miniature underwater sensor networks). The targeted full scale sea state in this work is the 20 year average for RI shelf waters (south of Block Island), which provides a modest  $J = 3.2$  KW/m of wave crest, for a significant wave height  $H_s = 1.2$  m and peak spectral period  $T_p = 4.5$  s (with  $J \simeq \rho g^2 H_s^2 T_p / (64\pi)$  according to linear wave theory; Dean and Dalrymple, 1984; Previsic et al., 2004).

Several buoy design alternatives were evaluated, through a combination of theoretical analyses and numerical simulations for periodic or irregular waves. This led to selecting two buoy designs (referred to as DC2 and DC3; Figs. 1, 2) and optimizing their parameters. Based on these analyses, 1:10 scale models of

both designs were built and tested in URI's wavetank (Figs. 3, 4), and numerical models were calibrated based on experimental results and used to design ruggedized mini-prototypes of each design, at a larger 1:4 scale. These were field tested in Narragansett Bay, RI under properly scaled wave climates (e.g., Fig. 2c).

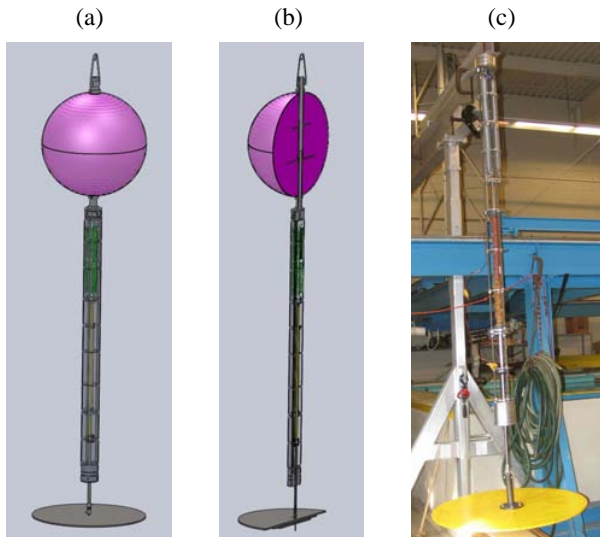


Fig. 1 : Wave energy buoy DC2: (a,b) Solidworks drawings; (c) partial assembly of 1/4 scale mini-prototype.

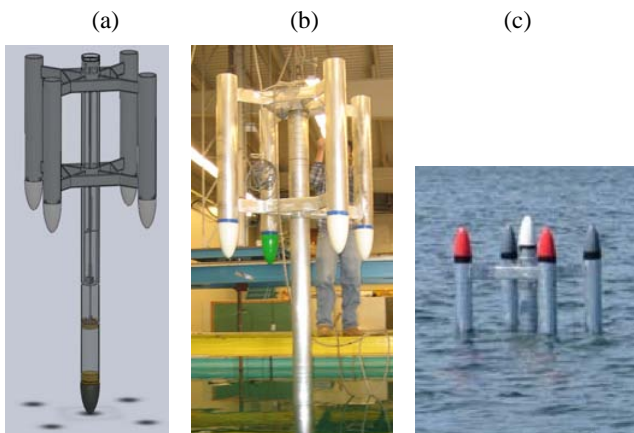


Fig. 2 : Wave energy buoy DC3: (a) Solidworks drawings; (b) static testing of 1/4 scale mini-prototype partial assembly; (c) ocean testing of the latter.

In both systems, wave mechanical energy induces buoy motion, which then produce electricity by way of the coupled oscillations of a Linear Electric Generator (LEG) located in a central spar buoy/canister (Figs. 1,2). The LEG is simply made of a permanent magnet, suspended to a spring, oscillating within a (two-phase) coil (e.g., the coil, magnetic armature and springs visible on Fig. 1c). In all cases, the main mode of wave energy harvesting is heave motion, with secondary roll oscillations.

More specifically, in the buoy system referred to as DC2 (Fig. 1), a spherical float, to which a cylindrical canister is rigidly attached, oscillates on the surface and forces the motion of a LEG,

which is housed and suspended within a cylindrical (spar buoy) canister. A rod, attached to the LEG magnetic armature, exits through the bottom of the canister and connects to a large submerged resistance platform (which also serves as ballast), by way of a universal joint. The differential motion between the phase shifted float and platform motions drives the LEG oscillations.

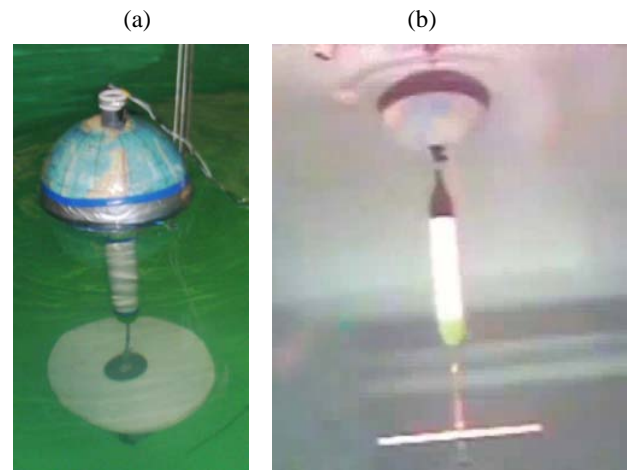


Fig. 3 : 1:10 scale model of DC2 wave energy buoy in wavetank testing: (a) View from above the water; (c) Underwater view taken with mini-ROV.

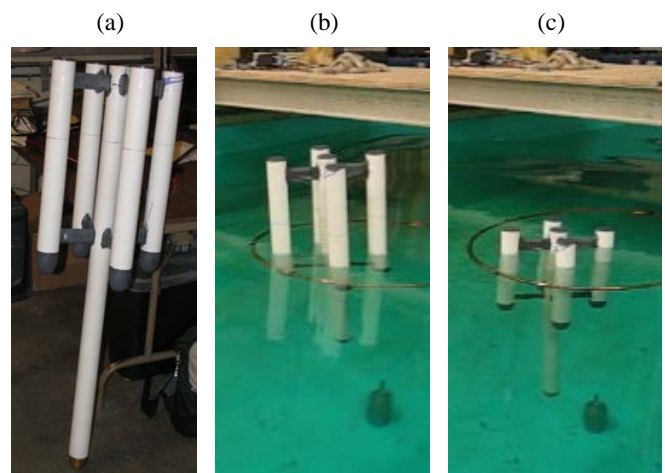


Fig. 4 : 1:10 scale model of DC3 wave energy buoy in wavetank testing: (a) View of model on dry land; (b/c) Model tested at resonance peak/maximum submergence in periodic waves.

By contrast, the system referred to as DC3 (Fig. 2) is a self-contained (water tight) resonating (e.g., Budal and Falnes, 1975) multiple-spar buoy (or *Starspar*), in which the longer central spar is surrounded by shallower, satellite spars, providing both form stability and a reduced overall average draft of the system (necessary to achieve a proper heave resonance period). In DC3, the LEG is housed and suspended within the longer central spar, and has a massive ballast simply suspended to the bottom of its magnetic armature. Here, the LEG oscillations are forced by the entire buoy heave motion, through coupled resonance. Hence, to maximize

the buoy and LEG oscillations, both the starspar average draft and the LEG spring stiffness are selected for the systems heave resonance period to be near that of both the LEG and the targeted sea state peak spectral period (French, 1979).

In the following, we present an overview of the development and validation of analytical/numerical models of coupled buoy heave-(roll) and LEG mechanical motions, with some considerations for generator electro-magnetic circuits. Additionally, we present selected results of experimental calibration/validations and mini-prototype field testing, for some of the designs. Note that earlier work on a multiple spar design, precursor of DC3, was reported by Grilli et al. (2007) (this work also includes a short literature review and background on point-absorber types of wave energy buoy systems; see also Previsic et al., 2004), and work on the LEG and its specific circuit for optimizing electricity production and storing was presented by Bastien et al. (2009).

Three major, linked sub-systems, are considered in each buoy design, the: (i) *floating buoy dynamics* under wave action (i.e., heave, roll, . . .); (ii) *LEG dynamics* resulting from buoy motions (i.e., magnetic armature motion relative to the coils); and (iii) *LEG electric dynamics* (i.e., LEG electrical power output given the armature-coil dynamics). In the most general case, feedback between sub-systems must be considered to optimize the buoy system’s overall performance. As an example, the movement of the armature will result in a change of the weight distribution and hence impact buoy motion. Similarly the electro-magnetic force from the armature-coil system will alter the mechanical response of the generator (a first-order effect to be considered, since the work of this force directly translates into electric energy production). In this paper, the focus has been restricted to the buoy and mechanical LEG dynamics portions of the problem (i.e., sub-systems (i) and (ii)), and the electric system (iii) is simply represented as a two-phase resistive circuit. More advanced considerations and details of our proposed electric circuit/system can be found in Bastien et al. (2009).

In the laboratory testing part of this work, the 1:10 scale buoy models were also equipped with small LEGs, with two-phase (essentially) resistive circuits, that matched the idealized representation used here, while in the field testing of the 1:4 mini-prototypes, larger LEGs with complete circuit boards were used, which were developed and built by ESL on the basis of their proprietary “quantum loading” algorithm. As an illustration, Fig. 5 shows electric parameters measured in dry testing, on the DC2 1:4 scale system shown in Fig. 1, as a function of time, in response to an initial armature displacement  $z_a \simeq 6.3$  cm, with the LEG circuits being either unloaded ( $n$ ) or loaded ( $l$ ) using a 5 Ohm resistor : rectified voltage  $V_{n,l}$ , current  $i_l$ , and power  $P_l$ . The method of rectification uses a two-phase rectifier bridge, which combines both phases into one output (i.e., one circuit load), but the net effect on the mechanical system is not too different than having simple separate and isolated resistors on each phase. In this test, the bottom platform was released at  $t = 0$  s, after which its motion decayed over 5 subsequent oscillations, as a result of the LEG electro-mechanical force and/or mechanical friction; while a voltage is generated, no current circulates when the circuits are unloaded and hence no electro-mechanical damping force occurs, yielding larger ampli-

tude oscillations. For the (loaded) data shown in Fig. 5, a maximum of about 2 W of power was generated during the maximum platform oscillation of 6 cm amplitude. Maximum power generation occurs, as expected, whenever the armature velocity is maximum, i.e., at about  $z_a = 0$ . Finally, the mechanical system is seen to freely oscillate at its constant natural period, whether loaded or unloaded, which is measured at  $T_s = 1.083$  s (this will be further discussed later).

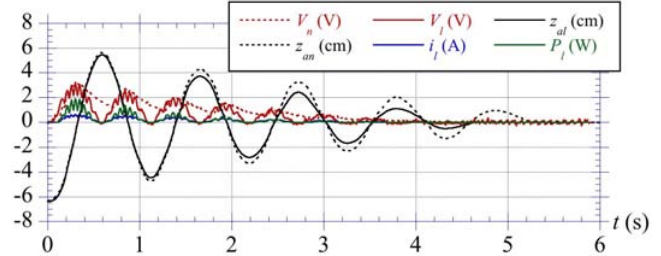


Fig. 5 : Electric parameters (voltage  $V$ , current  $i$ , power  $P$ ) measured on the DC2 1:4 scale system, shown in Fig. 1, as a function of time, in response to initial armature displacement  $z_a$ . The two-phase circuits were either unloaded (subscript  $n$ ) or loaded (subscript  $l$ ) using a 5 Ohm resistor.

The main aim of this work was to maximize power production by tuning the response of sub-systems (i) and (ii) to wave forcing. The goal is to select parameters so that the mechanical responses of the buoy and the LEG are maximized for the most prevalent wave conditions. Ideally, in accordance with typical ocean wave energy spectra, the buoy systems should have broadband response such as to optimize wave energy capture over a range of wave frequencies, and not just at or near one fixed frequency. While the non-resonating DC2 exhibits a reasonably large band response, DC3 is tuned to resonate at and near a specific wave period. Such resonant systems, however, could be further tuned to improve their response through fixed, slow, or fast tuning. Fixed tuning refers to non-changeable properties of the device (i.e., size, shape, and mass). Slow tuning refers to changes in the response on time scales of minutes to hours and typically is focused on changing the systems buoyancy and hence its mass and effective stiffness. This can be achieved for instance by active ballast control. Fast tuning actively controls system dynamics on the time scales of variation of individual waves or wave groups. The latter tuning is typically very difficult to implement because device characteristics must be changed quickly enough to alter its response. Also, for typical irregular sea states, one cannot exactly predict waves that are about to reach the system (and thus dynamically tune it for such waves), and hence one can only make a forecast and iteratively correct it over a number of wave periods (e.g., Babarit and Clément, 2006). In the present work, we only explored fixed tuning of each type of systems.

## THE ANALYTICAL AND NUMERICAL MODELS

### LEG Mechanical Design and Dynamics

The motion of the LEG spring-magnet, expressed by the ax-

ial displacement  $z_a(t)$  (in the canister direction  $\alpha$ ) of the magnetic armature relative to the coil/stator (which is attached to the buoy) from its initial static equilibrium, is classically described by a 2nd-order Ordinary Differential Equation (ODE). For an armature of mass  $M_g$  (including half of the spring mass and ballast), suspended to a spring of stiffness  $K_s$ , this equation has inertia, damping proportional to armature speed, and spring restoring terms in the left-hand-side, and is forced in the right hand side by the inertia force induced by the buoy acceleration  $\ddot{z}_b$  in the direction  $\alpha$  (upper dots are time derivatives; see details later). Additionally, for DC2, an excitation force  $\Delta F_p = F_p(t) - F_{p0}$  caused by the platform motion is included (also detailed later), where  $F_{p0}$  denotes the platform weight underwater projected in direction  $\alpha$ . We have,

$$M_g \ddot{z}_a + \mu \dot{z}_a + K_s z_a = \Delta F_p - M_g \ddot{z}_b \quad (1)$$

with  $\mu = \mu_g + \mu_f$  the LEG damping coefficient, combining an electromagnetic resistance coefficient  $\mu_g$  and friction coefficient  $\mu_f$ . In static equilibrium, the LEG spring has an initial extension,

$$l_{s0} = \frac{M_g g + F_{p0} - T_0}{K_s} ; F_{p0} = \frac{g(M_p - \rho_w \nabla_p)}{\cos \alpha} \quad (2)$$

assuming a spring preconstraint  $T_0$  (where, for DC3  $F_{p0} = 0$ ), a platform mass  $M_p = \rho_p \nabla_p$ , with  $\rho_w$  and  $\rho_p$  the water and platform density, respectively, and  $\nabla_p$  the platform volume.

Solving Eq. (1), with  $z_a = \dot{z}_a = 0$  at time  $t = 0$ , for a harmonic forcing with acceleration of amplitude  $a_o A$  (to simplify the algebra) and frequency  $\omega$  in the right-hand-side, and assuming dry testing in the vertical direction  $\alpha = 0$  in the case of DC2 (Fig. 1, i.e.,  $F_p = M_p(g - \ddot{z}_a)$ ;  $F_{p0} = M_p g$ ), we find the LEG Response Amplitude Operator (RAO)  $R = |z_a|/A$  as,

$$R = a_o \left\{ \{K_s - \omega^2(M_g + M_p)\}^2 + \omega^2 \mu^2 \right\}^{-\frac{1}{2}} \quad (3)$$

For this simple harmonic oscillator, maximum response  $R^{max} = a_o/(\omega \mu)$  occurs at the system's natural frequency,

$$\omega = \sqrt{\frac{K_s}{(M_g + M_p)}} = \sqrt{\frac{g}{l_{s0} + (T_0/K_s)}} = \omega_s \quad (4)$$

Hence, the longer the spring initial extension, the lower the LEG natural frequency. For the LEG used in the 1:4 scale DC2 prototype, for instance (Fig. 1), we have by design:  $T_0 = 156.48$  N and  $K_s = 3787.13$  N/m (both measured through a static loading experiment for the system of 6 springs used in the model),  $M_g = 12.75$  kg (for armature, rod and various plates/hardware mass), and  $l_{s0} = 0.222$  m. Eq. (2) yields  $F_{p0} = 873.07$  N and, assuming an average sea water density  $\rho_w = 1,025$  kg/m<sup>3</sup> and a platform made of steel plates (with actual density measured at  $\rho_p = 7,897.08$  kg/m<sup>3</sup>), a volume  $\nabla_p = 0.01295$  m<sup>3</sup> and mass  $M_p = 102.27$  kg (the model platform is made of a 1 m diameter, 1.27 cm thick plate of 78.77 kg, with a second smaller plate attached under it, of 23.50 kg; Fig. 1c).

Now, for dry testing, Eq. (4) yields  $\omega_s = 5.74$  r/s and  $T_s = 1.095$  s, which is consistent with the Fig. 5 measurements. [Note,

because of the absence of water, the initial spring extension to use in the second Eq. (4) is slightly longer, at  $l_{s0} = 0.257$  m.]

Finally, the mechanical power extracted from the buoy motion is due to magnet motion and corresponds to the work per unit time of the magnet damping force  $\mu \dot{z}_a$ , i.e.,  $P_\mu(t) = \mu \dot{z}_a^2$ . The fraction of this power used to produce electricity is  $\mu_g/\mu$  (minus additional magnetic and heat (Joule) losses).

## Buoys Heave Dynamics

Based on standard linearized floating body dynamics (e.g., Newman, 1977), in transient waves, when roll/pitch oscillations are small, the heave motion,  $\xi_3(t)$ , of both DC2 and DC3 buoys, in water of density  $\rho_w$  and depth  $h$ , is found from the conservation of linear momentum, based on inertia, radiative wave damping, viscous damping, gravity, and buoyancy forces, which is expressed as a 2nd-order nonlinear ODE as,

$$(M_b + a_{33}(\infty)) \ddot{\xi}_3 + \int_0^t \mathcal{K}_{b3}(t - \tau) \dot{\xi}_3(\tau) d\tau + b_{f,33} |\dot{\xi}'_3| \dot{\xi}'_3 + F_{bs} = F_3 + F_g - F_{35} \quad (5)$$

with  $M_b = \rho_w \nabla_{bo}$  the buoy mass, equal to the statically displaced water volume  $\nabla_{bo}$ ,  $a_{33}(\infty)$  the instantaneous added mass (for very large frequency),  $b_{f,33} = (1/2) \rho_w S_o C_{dh}$  the buoy heave viscous damping coefficient (with  $C_{dh}$  the buoy heave drag coefficient),  $\dot{\xi}'_3 = \dot{\xi}_3 - \tilde{w}$  (with  $\tilde{w}$  the wave vertical particle velocity at the buoy equivalent draft  $\tilde{d}$ ),  $F_{bs}(t) = \rho_w g \{ \nabla_b(\xi_3(t)) - \nabla_{bo} \}$  the heave buoyancy restoring force (equal to  $c_{33} \xi_3$  with  $c_{33} = \rho_w g S_o$  and  $S_o$  the total buoy horizontal cross-section for the starspar DC3 buoy),  $F_3(t)$  the wave heave excitation force, and  $F_g(t) = \mu \dot{z}_a + K_s z_a$ , the LEG reaction force on the buoy, function of the armature oscillator motion. The last term  $F_{35}(t)$  is a change in heave excitation and/or viscous damping due to the buoy roll/pitch oscillations, detailed later.

Assuming that the sea-state is made of the superposition of  $N$  linear periodic waves of amplitude  $A_n$  and frequency  $\omega_n$ , with energy density represented by the frequency spectrum  $S(\omega)$  (e.g., JONSWAP; JS), the incident wave elevation and vertical particle velocity at the equivalent draft, can be expressed as,

$$\eta(t) = \sum_{n=1}^N A_n \cos(\omega_n t + \psi_n) ; \frac{\omega_n}{g} = k_n \tanh k_n h \quad (6)$$

$$\tilde{w}(t) = \sum_{n=1}^N -A_n \omega_n \frac{\sinh k_n (h - \tilde{d})}{\sinh k_n h} \sin(\omega_n t + \psi_n) \quad (7)$$

where  $A_n = \sqrt{2S(\omega_n)\Delta\omega}$  (with  $\Delta\omega$  a small frequency interval),  $\psi_n \in [0, 2\pi]$  is a specified set of random phases, and the second Eq. (6) is the linear dispersion relationship expressing the wavenumber  $k_n$  for each wave component. Accordingly, the total wave heave excitation force reads,

$$F_3(t) = \rho_w g \sum_{n=1}^N A_n r_{3n} \cos(\omega_n t + \phi_{3n} + \psi_n) \quad (8)$$

where  $\{r_{3n}(\omega_n), \phi_{3n}(\omega_n)\}$  are the module and phase, respectively, of the heave exciting force caused on the buoy by a wave of unit amplitude and frequency  $\omega_n$  (including diffraction effects induced by the buoy).

**Heave Memory Term** The integral in Eq. (5) is a memory term (e.g., Babarit et al., 2006) expressing radiative wave damping, in which the heave impulse response function,  $\mathcal{K}_{b3}(t)$ , can be calculated as a function of the buoy frequency response by either of the inverse Fourier transforms,

$$\begin{aligned}\mathcal{K}_{b3}(t) &= -\frac{2}{\pi} \int_0^\infty (a_{33}(\omega) - a_{33}(\infty)) \omega \sin \omega t \, d\omega \\ &= \frac{2}{\pi} \int_0^\infty b_{33}(\omega) \cos \omega t \, d\omega\end{aligned}\quad (9)$$

as a function of  $a_{33}(\omega)$  and  $b_{33}(\omega)$ , the buoy frequency dependent heave added mass and wave radiative damping coefficients, respectively. The memory term is expressed as a time convolution in Eq. (5), which is both costly and difficult to accurately evaluate at each time, in the numerical solution of Eq. (5). This difficulty can be overcome by representing  $\mathcal{K}_{b3}$  by way of the Prony method, which transforms the convolution into a system of additional ODEs for the Prony coefficient (e.g., Babarit and Clement, 2006) as,

$$\begin{aligned}\mathcal{K}_{b3}(t) &= \sum_{p=1}^{N_p} \beta_{3p} \exp(S_{3p}t) \\ \int_0^t \mathcal{K}_{b3}(t-\tau) \dot{\xi}_3(\tau) \, d\tau &= \sum_{p=1}^{N_p} \beta_{3p} I_{3p}(\dot{\xi}_3, t) \\ \dot{I}_{3p} &= S_{3p} I_{3p} + \dot{\xi}_3 \quad ; \quad p = 1, \dots, N_p\end{aligned}\quad (10)$$

where  $(\beta_{3p}, S_{3p})$  are  $N_p$  complex coefficients (typically 4 for the relatively simple geometries of DC2 and DC3), which are found through Prony's "curve fitting".

**Linearized Heave Solution for Periodic Waves** As indicated before, DC2 and DC3's frequency dependent wave coefficients  $\{a_{33}, b_{33}, r_3, \phi_3\}$  are calculated using the standard Boundary Element code WAMIT (Lee, 1995; Newman, 1977), in which *linearized* free surface boundary conditions are specified. Thus, for given buoy geometry and mass distribution, WAMIT computes results for  $N$  equally spaced periods  $T_n$  (with  $\omega_n = 2\pi/T_n$ ), in a specified interval  $(T_{min}, T_{max})$ .

For periodic incident waves of amplitude  $A$  and frequency  $\omega$ , similar to Eq. (5), *linearized* (complex) equations governing buoy motion for each of 6 degrees of freedom can be expressed using these coefficients (e.g., Newman, 1977) as (assuming tensor notation's summation convention),

$$\left\{ -\omega^2(M_{ml} + a_{ml}) + i\omega(b_{ml} + b'_{f,ml}) + c_{ml} \right\} \xi_l = A r_l e^{i\psi_l}$$

with  $\xi_l$  the complex buoy amplitude in direction  $l$ . In this equation,  $b'_{f,ml}$  denotes the *linearized* friction coefficient obtained by applying the principle of "equivalent average dissipated power" over one wave period (e.g., Berteaux, 1994). For the linearized heave motion ( $l = 3$ ) of multiply symmetric bodies ( $a_{m3} = b_{m3} = 0$

for  $m \neq 3$ ), with  $M = M_{33} = M_b + M_g + M_p$ , and  $b'_{f,33} = \{8 |\zeta_3| \omega / (3\pi)\} b_{f,33}$ , this equation yields the heave frequency dependent Response Amplitude Operator (RAO)  $Z_3 = |\zeta_3|/A$  as,

$$Z_3 = r_3 \left\{ c_{33} - \omega^2(M + a_{33})^2 + \omega^2(b_{33} + b'_{f,33})^2 \right\}^{-\frac{1}{2}} \quad (11)$$

This equation predicts maximum heave response  $Z_3^{max} = r_3 / \{\omega(b_{33} + b'_{f,33})\}$  when incident waves occur at the heave natural frequency,

$$\omega = \sqrt{\frac{c_{33}}{M + a_{33}(\omega)}} = \omega_H = \frac{2\pi}{T_H} \quad (12)$$

Eq. (11) also shows that, in the absence of viscous damping ( $b'_{f,33} = 0$ ; such as assumed in WAMIT) and for a very small value of the linear wave damping coefficient  $b_{33}$  (as, e.g., for the starspar buoy DC3), maximum heave response will be significantly over-predicted near resonance. Hence, when solving Eqs. (5) to (10) one needs to use a properly calibrated drag coefficient  $C_{dh}$  for the buoys, which can be obtained through a comparison of model prediction with laboratory measurements performed on a scale model (e.g., Figs. 3,4).

**Multiple Spar Buoys** As indicated, for slender spar buoys, such as the components of the starspar DC3,  $a_{33}$  is small and varies little over any useful frequency interval around the buoy's heave resonance frequency, while  $b_{33}$  is very small, reflecting the fact that such buoys generate little waves in heaving motion (Grilli et al., 2007). Thus, Eqs. (9) yield  $\mathcal{K}_{b3}(t) \simeq 0$ , and hence the memory/radiative wave damping term in Eq. (5) is negligible, particularly as compared to the viscous damping term.

Additionally, the starspar is made of  $N_s + 1$  rigidly connected vertical spar buoys of cylindrical shape, draft  $d_i$ , external diameter  $D_i$ , and total length  $\ell_i$  (Fig. 2) ( $i = 1, \dots, N_s + 1$ ). The individual buoys are set sufficiently apart (typically a couple of diameters) not to interact hydrodynamically in heave. The submerged extremity of each buoy is streamlined to reduce friction drag generated during motion (Fig. 2; this slight change of geometry is neglected in the following idealized analysis). Due to the small added mass Eq. (12) predicts the starspar natural heave period as,

$$T_H \simeq 2\pi \sqrt{\frac{M}{c_{33}}} = 2\pi \sqrt{\frac{\tilde{d}}{g}} \quad \text{with} \quad \tilde{d} = \frac{\sum_{i=1}^{N_s+1} S_i d_i}{\sum_{i=1}^{N_s+1} S_i} \quad (13)$$

the buoy equivalent draft; we also find  $S_o = \sum_{i=1}^{N_s+1} S_i$  in the heave buoyancy restoring term  $c_{33} = \rho_w g S_o$  with  $S_i = \pi D_i^2/4$ , each spar buoy's cross-section. Grilli et al. (2007) numerically verified that this equation is accurate for  $D_i/d_i < 0.1$ .

**Buoy Roll/pitch Dynamics** The buoy's roll (or pitch, identical for buoys with two axes of symmetry) angular motion  $\xi_5 = \alpha(t)$  is modeled, similarly to heave as,

$$(I_{55} + a_{55}(\infty)) \ddot{\alpha} + \sum_{p=1}^{N_p} \beta_{5p} I_{5p}(\dot{\alpha}, t) + M_{f,53} + c_{55} \sin \alpha = M_5$$

$$\dot{I}_{5p} = S_{5p} I_{5p} + \dot{\alpha} \quad ; \quad p = 1, \dots, N_p$$

$$M_5(t) = \rho_w g \sum_{n=1}^N A_n r_{5n} \cos(\omega_n t + \phi_{5n} + \psi_n) \quad (14)$$

where  $I_{55}$  and  $a_{55}$  are the mass moment of inertia and added inertia, respectively, the second term expresses (linear) radiative wave damping,  $M_{f,53}$  is the viscous damping moment resulting from heave-roll interactions (detailed below),  $c_{55} = (M_b + M_g + M_p) g \overline{GM}$ , is the roll (or pitch) restoring moment (with  $\overline{GM}$  the metacentric distance), and  $M_5$  is the wave roll excitation moment calculated by superposition of wave forcing, as for heave.

For DC2, the wave excitation moment in roll is zero on the spherical float. However, when the buoy is moored below the float to prevent drifting, there is significant roll (as, e.g., seen in laboratory experiments) as a result of the float's sway (i.e.,  $x$ ) oscillations and the non-uniform mass distribution in the buoy (the massive platform is located at the bottom). Rather than modeling the complicated geometry of DC2 in WAMIT, we instead estimated roll parameters used in Eq. (14) based on buoy sway motion  $\xi_1$  as,

$$\begin{aligned} \alpha &= \xi_1 / \overline{OR} \quad ; \quad a_{55}(\infty) \simeq a_1(\infty) \overline{OR}^2 \\ \sum_{p=1}^{N_p} \beta_{5p} I_{5p}(\dot{\alpha}, t) &\simeq \overline{OR}^2 \cos \alpha \sum_{p=1}^{N_p} \beta_{1p} I_{1p}(\dot{\alpha}, t) \\ \dot{I}_{1p} &= S_{1p} I_{1p} + \dot{\alpha} \quad ; \quad p = 1, \dots, N_p \\ M_{f,53} &\simeq b_{f,11} \overline{OR}^3 |\dot{\alpha}'| \dot{\alpha}' \cos \alpha \\ M_5 &\simeq (F_1 - F_g \sin \alpha) \overline{OR} \cos \alpha \end{aligned} \quad (15)$$

where  $\dot{\alpha}' = \dot{\alpha} - u_b / \overline{OR}$  (with  $u_b$  the wave particle velocity at buoy draft, calculated with an equation similar to (7)),  $b_{f,11} = (1/2) \rho_w S_o C_{ds}$  the buoy sway viscous damping coefficient,  $\overline{OR}$  denotes the distance between the center of the buoy water plane  $O$  on the surface and the center of rotation  $R$ , and the Prony coefficients are calculated using the float's sway impulse response function,  $\mathcal{K}_{b1}(t)$ , similar to Eqs. (9) and (10). For DC2, in view of the larger viscous drag of the spherical float, as compared to the spar canister, we assume  $F_{35} \simeq 0$  in the buoy Eq. (5). Finally, in Eq. (1), as a result of the buoy's heave, sway and roll, the LEG motion is excited by the acceleration,

$$\ddot{z}_b = \ddot{\xi}_1 \sin \alpha + \ddot{\xi}_3 \cos \alpha + \dot{\alpha}^2 \frac{M_b}{M_g} \overline{OR} \quad (16)$$

where the last term is an additional excitation of the LEG resulting from the centrifugal acceleration caused by the buoy roll motion.

For the DC3 starspar, we simply calculate the full WAMIT coefficients for roll  $\{a_{55}, b_{55}, r_5, \phi_5\}$ , from which we calculate the roll excitation  $M_5$  using Eq. (14) and the radiative damping term, as expressed in the same equation, by applying the Prony method to the roll impulse response function  $\mathcal{K}_{b5}(t)$  calculated similarly to Eqs. (9) and (10) for heave.

**Platform dynamics for DC2 buoy** Although, in DC2's buoy, the platform is connected to the LEG rod through a universal (U) joint (Fig. 1c), in the modeling, it is treated as a separate rigid body with vertical (heave) motion  $z_p$ , relative to the buoy heave motion  $\xi_3$ ,

from its initial static equilibrium location. The U-joint is assumed to have a large but finite stiffness  $K_u$  and, hence, assuming the buoy canister is angled by  $\alpha$ , the force acting on the rod, parallel to it is,

$$F_p = \frac{1}{\cos \alpha} \{ (M_p - \rho_w \nabla_p) g + K_u (z_a \cos \alpha - z_p) \} \quad (17)$$

Assuming a balance between inertia, gravity, and viscous drag forces, but no direct wave excitation due to the deep submergence, the platform equation of motion reads,

$$M_p' \ddot{z}_p + b_{fp} |z_p'| z_p' + K_u z_p = \{ K_u z_a + M_p \overline{RP} \dot{\alpha}^2 \} \cos \alpha - M_p' \ddot{\xi}_3 \quad (18)$$

where  $M_p' = M_p + M_{pa}$ , the platform virtual mass, includes a constant added mass  $M_{pa} = (1/3) \rho_w D_p^3$  (for a thin circular plate),  $b_{fp} = (1/2) \rho_w S_p C_{dp}$  the platform heave viscous damping coefficient, with  $C_{dp} = 8 / (K C_p)^{1/3}$  the platform drag coefficient for a thin circular plate ( $K C_p = 2\pi A_s / D_p$  is the platform Keulegan

Carpenter number), with  $z_p' = \dot{\xi}_3 + \dot{z}_p - w_p$  (where the latter is the wave vertical particle velocity at the mean platform depth  $h_p$ , from Eq. (7)). A centrifugal excitation force is included in the right hand side, as a function of roll velocity and distance from the platform to the rotation center  $\overline{RP}$ . Now, for the 1:4 scale DC2 buoy, in view of the platform added mass  $M_{pa} = 333.33$  kg, the resonance period of the LEG/platform system in the water becomes, from Eq. (4),  $T_s = 2.13$  s, which is close to the targeted wave period at this scale ( $T_p = 2.25$  s based on Froude scaling).

**Solution** WAMIT is first run for the selected buoy geometries and mass distribution, to calculate the heave, sway, and roll frequency domain coefficients. The LEG dynamics and buoy heave/roll coupled equations are then solved in the time domain on the basis of general data and these coefficients. After being transformed into two 1st-order ODEs by change of variables, the nonlinear 2nd-order ODEs of the type (10), (14), and (15), for  $l = 3, 5$  or 1 respectively, depending on the case, are time integrated by a Runge-Kutta method; for DC2, assuming  $N_p = 4$ , this represents a system of 22 coupled ODEs. Initial conditions are simply set by assuming all variables to be zero for  $t = 0$ . Computations are usually pursued up to at least  $t = 150 T_p$ , for the given wave energy spectrum. If the buoy is subjected to periodic waves only, the same equations are solved from an initial state of rest, assuming  $N = 1$ , until the transient buoy motion reaches a periodic state.

## APPLICATIONS

As indicated, we performed laboratory experiments on 1:10 scale models of the DC2 and DC3 buoys (in periodic or irregular waves; Fig. 3 and 4), in URI's 30 m long, 3.6 m wide and 1.8 m deep wavetank, in order to: (i) both verify and quantify the expected model behavior in terms of buoy dynamics in waves, LEG motion, and electric power production; (ii) calibrate friction drag coefficients  $C_{dh}$  and  $C_{ds}$ , for the numerical models detailed above to closely simulate experimental results. Following this

experimental/numerical approach, the calibrated numerical model were used to design ruggedized 1:4 scale mini-prototypes of both design, which were (or will be) field tested (Figs. 1 and 2). According to Froude scaling, for the targeted field conditions, the targeted sea state parameters are  $H_s = 0.12, 0.3$  m and  $T_p = 1.42, 2.25$  s, for 1:10 and 1:4 scales, respectively.

In laboratory experiments, a computer-controlled wavemaker is used to generate waves and capacitance gages are used to measure surface elevation near the buoys. A mildly sloping beach, located over the last 20 m of the tank, causes incident wave breaking and reduces wave reflection in the tank to a very small level. The buoy models are placed in the deeper water region in front of the slope and prevented from drifting by either a long horizontal mooring line (DC2) or a fixed plastic ring (DC3). In field testing, which took place in nearby Narragansett Bay, RI (in which the targeted sea state is usually observed for episodes of NE wind blowing at 9-10 m/s, for 4-5 hrs or so), the mini-prototypes were free-drifting and a waverider buoy was deployed near the buoys to measure sea state. In both laboratory and field testing, three-axis (WIFI) accelerometers were mounted within the buoy models. For DC2, two of these measured both float and platform motion and, for DC3, three of those measured the central spar and two satellite spar motions. Additionally, voltage and other electric parameters are recorded during tests for the 2 phases of the LEG, and for the prototype, Hall effect sensors record the motion of the magnetic armature.

Due to lack of space, in this paper, we only report in detail on laboratory experiments and modeling of the DC2 buoy. Preliminary work on the multiple-spar concept was presented in Grilli et al. (2007) and details of experiments and modeling of the DC3 starspar buoy can be found in Grilli et al. (2010).

### Laboratory Testing and Modeling of DC2 Scale Model

The 1:10 DC2 scale model (Fig. 3) was tested in the wavetank for a series of periodic and irregular sea states. This model has a spherical float of diameter  $D_b = 0.305$  m, draft  $d_b = 0.150$  m and mass  $M_b = 2.067$  kg, including the 0.883 kg mass of the LEG canister (including half spring and LEG stator mass) of length  $h_c = 0.451$  m and diameter  $D_c = 0.051$  m, a platform of diameter  $D_p = 0.4$  m, thickness  $t_p = 0.0145$  m and mass  $M_{p0} = 1.917$  kg (Volume  $V_{p0} = 1.8222 \cdot 10^{-3} \text{ m}^3$ ). Unlike in the 1:4 prototype, in this scale model, a spherical ballast is suspended below the platform, with volume  $V_{ba} = 1.3776 \cdot 10^{-3} \text{ m}^3$  and mass  $M_{ba} = 7.708$  kg. This yields for the platform plus ballast, a total volume  $V_p = V_{p0} + V_{ba} = 3.1998 \cdot 10^{-3} \text{ m}^3$  and mass  $M_p = M_{p0} + M_{ba} = 9.625$  kg. Hence, the 2nd Eq. (2) yields  $F_{p0} = 64.39$  N. A small LEG was fabricated at scale, for which  $M_g = 0.144$  kg, for the armature, rod, and half spring mass. The LEG spring stiffness was measured at  $K_s = 1107.96$  N/m and initial tension at  $T_0 = 11.78$  N. In this small model, stiction caused by the seal at the bottom of the canister, was found to be relatively larger than in the 1:4 scale prototype, and measured at  $S_0 = 5.4$  N; this value must be subtracted from  $F_{p0}$ . Based on this data, and using the fresh water density  $\rho_w = 1,000 \text{ kg/m}^3$  in the wavetank, the 1st Eq. (2) yields the initial spring extension

$l_{s0} = 0.0427$  m in the water. [For dry testing in the air, this extension would increase to  $l_{s0} = 0.071$ , with Eq. (4) yielding a resonance period  $T_s = 0.59$  s.] The platform added mass is  $M_{pa} = 21.33$  kg; hence, adding the latter to the platform mass in the water, we find with Eq. (4), the LEG resonance period in the water  $T_s = 1.00$  s.

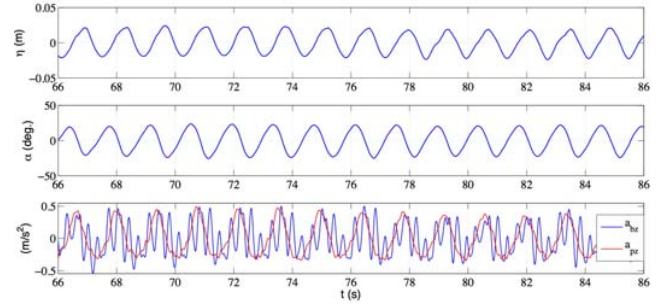


Fig. 6 : Measurements for DC2 1:10 scale model (Fig. 3) experiments in periodic waves, with  $\bar{H} = 0.042$  m and  $\bar{T} = 1.38$  s: (top) wave gage elevation  $\eta$ ; (middle) roll angle  $\alpha$  calculated from float horizontal acceleration; (bottom) vertical float (blue,  $a_{bz}$ ) and platform (red,  $a_{pz}$ ) acceleration.

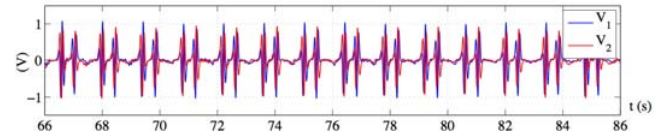


Fig. 7: Same case as Fig. 6. Voltage generated on each of the LEG two phases (loaded with a  $R_L = 10$  Ohm resistor) .

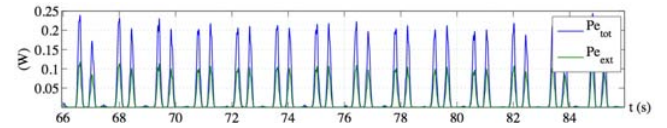


Fig. 8: Same case as Figs. 6,7 Total electric power dissipated ( $P_{e_{tot}}$ ); electric power dissipated on external resistors ( $P_{e_{ext}}$ ).

Figures 6-8 show experimental results obtained in periodic waves of mean height  $\bar{H} = 0.042$  m and period  $\bar{T} = 1.38$  s, in water depth  $h = 1.35$  m. For periodic waves in deep water (here  $L_o/h = 2.2$ ), the incident average wave power is  $J \simeq \rho g^2 \bar{H}^2 \bar{T} / (32\pi) = 2.33$  W/m, which yields a buoy captured energy  $J D_b = 0.71$  W. Fig. 6 (top) shows that wave elevation measured near the buoy was reasonably sinusoidal and periodic. The induced float and platform vertical accelerations (bottom) are out of phase with the wave elevation, and with each other. While the platform acceleration is fairly monochromatic, the float acceleration has repeatable higher frequency oscillations, centered around a mean periodic oscillation (see details later). The buoy roll oscillations (middle) are seen to be closely periodic, but more sawtooth-like (likely due to the restoring force from the horizontal anchor line) and in opposition of phase with the wave elevation. Roll oscillations are between  $\pm 20$  deg., using  $OR = 0.326$  when processing the horizontal acceleration (Eq. (15)), in order for it to match observations. In view of periodicity, roll is simply obtained here as,  $\alpha(t) = \ddot{\alpha}(t)/\omega^2$ .

Fig. 7 shows the voltage generated on both phases of the LEG (when loaded with a  $R_L = 10$  Ohm resistor; while the internal resistance of each phase was  $R_S = 10$  Ohm as well), and Fig. 8 shows the corresponding electric power dissipated on the external resistors ( $P_{e_{ext}}$ ) or for the full circuit ( $P_{e_{tot}}$ ). The latter reaches a maximum of 0.2 W (or 28% of the incident captured wave power) while the former is about half that; we further find the average powers:  $\overline{P_{e_{tot}}} = 0.0376$  W (or 5.3% of incident captured wave power) and  $\overline{P_{e_{ext}}} = 0.0183$  W; for later comparisons, the RMS of the total dissipated power is  $P_{e_{tot},RMS} = 0.074$  W.

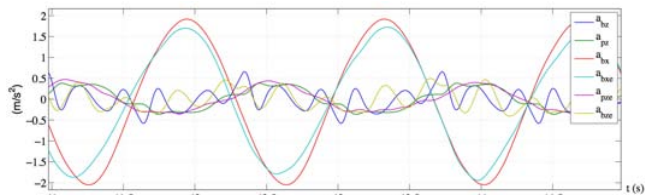


Fig. 9: Same case as Figs. 6-8. Comparison of experimental (e) and numerical results for float vert. accel. (blue,  $a_{bz}$ ; yellow,  $a_{bze}$ ) horiz. accel. (red,  $a_{bx}$ ; turquoise,  $a_{bx,e}$ ), platform vert. accel. (green,  $a_{pz}$ ; purple,  $a_{pze}$ ).

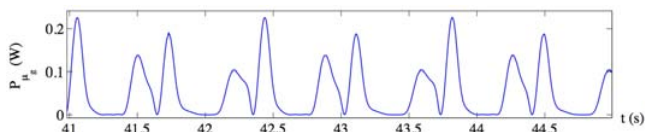


Fig. 10: Same case as Figs. 6-9. Mechanical power extracted by the LEG in numerical simulations.

Figures 9 and 10 show numerical simulation results for the DC2 1:10 scale model, based on equations detailed in the previous section. The only calibration done in the model was to specify,  $C_{dh} = C_{dh} = 1.5$  for the buoy drag and  $C_{dp} = 2.5$ , for the the platform drag, as well as adjusting the distance to the center of rotation  $\overline{OR}$  (as indicated above). Fig. 9 shows, there is good agreement between measured and simulated vertical platform and horizontal float, accelerations. The lower frequency variation is also in good agreement for the float vertical acceleration. However, to satisfactorily reproduce the measured higher frequency modulations, we had to introduce a phase shift in the electro-mechanical forces caused by both phases of the small custom LEG, which is likely due to imperfections in its winding (a perfectly wound 2 phase LEG is devoid of such modulations, as can be seen, e.g., in Fig. 5 in the smooth motion of the 1:4 scale DC2 buoy in free oscillations). Since the exact nature of these imperfections is unknown, the high frequency oscillations are only approximately reproduced in the model. Fig. 10 shows the predicted mechanical power,  $P_{\mu_g} = \mu_g \dot{z}_a$  extracted by the LEG in numerical simulations, which is to be compared to the measured total dissipated electric power  $P_{e_{ext}}$  in Fig. 8. Although there are differences in their time series (related to differences in the modeling of small high frequency oscillations of the float), both vary between 0.15-0.22 W; furthermore,  $P_{\mu_g,RMS} = 0.088$  W or 19% more than  $P_{e_{tot},RMS}$ , implying a (realistic) 83% efficiency of mechanical to electric power conversion in the LEG, due to

various magnetic losses and imperfect winding of the generator, which both affect the value of the LEG coefficient  $\mu_g$ .

## CONCLUSIONS

We tested and modeled two new types of wave energy buoy designs. For DC3, viscous friction is the dominant damping mechanism near resonance and rolling must be minimized, as it may significantly increase such damping; this is achieved by using satellite buoys. For DC2, the massive submerged platform both lowers the center of mass (thus increasing roll stability) and provides a reaction to the float motion. Finally, the phase difference in float-platform motion increases LEG oscillations and power production, as compared to a fixed anchor line.

## REFERENCES

- Babarit, A., and A. H. Clément, (2006) "Optimal latching control of a wave energy device in regular and irregular waves," *Applied Ocean Res.*, Vol 28, pp 77-91.
- Bastien, S.P., Sepe R.B., Grilli A.R., Grilli S.T., and M.L. Spaulding (2009) "Ocean Wave Energy Harvesting Buoy for Sensors," *Proc. IEEE Energy Conversion Congress and Exposition (ECCE09, San Jose CA, September, 2009)*, pps 3718-3725, doi: 978-1-4244-2893-9/09/.
- Berteaux, H.O, (1994) *Coastal and oceanographic buoy engineering*, H.O. Berteaux, Woods Hole, MA, 285pps.
- Budal, K. and J. Falnes (1975) "A resonant point absorber of ocean wave power," *Nature*, Vol 256, pp 478-479.
- Dean R. and R.A. Dalrymple (1984) *Water wave mechanics for engineers and scientists*, Prentice Hall Inc, New Jersey.
- French, M. J. (1979) "A generalized view of resonant energy transfer," *J. Mech. Engng. Science*, Vol 21, pp 299-300.
- Grilli, A., R., Merrill, J., Grilli S.T., Spaulding, M.L., and Cheung, J.T. (2007) "Experimental and numerical study of spar buoy-magnet/spring oscillators used as wave energy absorbers," *Proc. 17th Offshore and Polar Eng Conf*, Lisbon, ISOPE, Vol 1, pp 489-496.
- Grilli, A.R., Asher, T.G., Grilli, S.G. and M.L. Spaulding (2010) "Development of Renewable Energy Wave Powered Generator for Free Floating Ocean Buoy." *Technical Rept for "Rhode Island STAC Alliance"*, 72 pps.
- Lee, C.-H. (1995) *WAMIT Theory Manual*. MIT Rept 95-2, Dept. of Ocean Eng., MIT.
- Newman, J., (1977). *Marine Hydrodynamics*, MIT Press, Cambridge, MA (9th reprint).
- Previsic, M., R. Bedard, and G. Hagerman (2004). "Assessment offshore wave energy conversion devices," Rept No: E2I EPRI. WP-004-US-Rev 1. June 16, 2004

## ACKNOWLEDGEMENTS

This research was supported by STTR Phase I and II grants from the US Office of Naval Research, and by a grant from the State of Rhode Island STAC Alliance Program. The help of OCE technicians Fred Pease and Matt Jewell for building buoy scale models is gratefully acknowledge, as well as that of OCE seniors students, for helping to assemble and test the buoy models.